Turk. J. Math. Comput. Sci.
16(1)(2024) 199–205

DOI : 10.47000/tjmcs.1451966

Computational Investigation of Steady Incompressible Dilatant Flow in an Enclosed Cavity

Serpil Şahin

Department of Mathematics, Faculty of Science and Arts, Amasya University, 05000, Amasya, Turkey.

Received: 13-03-2024 • Accepted: 15-04-2024

Abstract. This paper presents a comprehensive investigation into the numerical solutions of two-dimensional incompressible dilatant flow in an enclosed cavity region. The continuity and momentum equations are solved using pseudo time derivative approach considering appropriate initial and boundary conditions. As a result, the equations governing flow motion are decomposed using the finite difference method and subsequently solved numerically. Numerical solutions are calculated up to a Reynolds number (Re) of 5000, using an extensive mesh. Based on the obtained results, it is evident that the method used proves to be both effective and highly accurate. Finally, we discuss the need for further research.

2020 AMS Classification: 76D05, 76M20

Keywords: Finite difference method, pseudo time derivative, dilatant fluids, numerical solution, Reynolds number.

1. Introduction

A non-Newtonian fluid is characterized by a nonlinear flow curve, where the relationship between shear stress and shear rate doesn't pass through the origin. In other words, its apparent viscosity, defined as shear stress divided by shear rate, varies with flow conditions such as geometry and shear rate, making it dependent on multiple factors, including temperature and pressure. The primary distinguishing feature of non-Newtonian fluids is their nonlinearity in how shear stress relates to shear rate. Due to changes in dynamic viscosity with shear stress, understanding and modeling the behavior of non-Newtonian fluids become notably complex. For this reason, the numerical solution of non-Newtonian fluids behavior demands special consideration [3, 4, 9, 14, 17, 21].

A specific type of non-Newtonian fluids is the dilatant fluid, also known as a shear-thickening fluid. In dilatant fluids, the apparent viscosity increases as the shear rate rises. A common example of this behavior is the mixture of cornstarch and water, often referred to as "oobleck". When subjected to sufficient force, oobleck hardens, enabling individuals to run across large pools filled with this intriguing mixture. A more relatable example can be found in wet sand. When you walk across it slowly, you'll notice yourself sinking gradually, but if you apply enough force, like running, the beach will solidify beneath your feet.

Extensive research has been conducted to explore the various applications of dilatant and non-Newtonian fluids. For such studies, Burggraf [2] investigated the Prandtl-Batchelor theorem in the context of a square cavity. Employing a relaxation, solutions were computed for Reynolds number (Re) up to 400. The results indicated the emergence of an inviscid core vortex for higher Re values, while secondary vortex was observed near the bottom corners of the cavity for all Re values. Sivakumar et al. [19] delved into the flow characteristics of power-law fluids passing an elliptic cylinder,

Email address: serpil.sahin@amasya.edu.tr (S. Şahin)
The author is supported by the Office of Scientific Research Projects Coordination at Amasya University, Grant number: FMB-BAP 15-0100.

scrutinizing both pseudoplastic and dilatant behavior. Ghia et al. [10] introduced a flow modeling approach utilizing the multigrid method, subsequently applying it to study shear-driven flow within a square cavity. Their investigation unveiled a variety of flow features, particularly for Reynolds number (Re) up to 10^4. Xu et al. [22] conducted flow analysis for Reynolds number (Re) ranging from 10 to 1000, while Khorasanizade and Sousa [13] extended their analysis to the range of Re from 400 to 3200, employing the newly developed Smoothed Particle Hydrodynamics (SPH) method.

Mahmood et al. [15] and Shuguang [18] employed the Carreau model to describe the power-law fluid behavior and conducted simulations within a square cavity. Mahmood et al. used the finite element method, while Shuguang employed the finite deference method. Their findings highlighted that the influence of the power-law index becomes increasingly significant at higher Reynolds number. Wright and Gaskell [20] applied the block implicit multigrid method (BIMM) to sharp and monotonic algorithm for realistic transport (SMART) and quadratic upstream interpolation for convective kinematics (QUICK) discretization schemes, presenting cavity flow results obtained on a 1024×1024 grid mesh for Reynolds number (Re) up to 1000. Nishida and Satofuka [16] introduced a novel higher order method for simulating driven cavity flow. They employed a modified differential quadrature (MDQ) method for discretizing the spatial derivatives of the Navier-Stokes equations, yielding high-order accurate solutions for Reynolds number (Re) up to 3200. Goyon [11] solved the stream function and vorticity equations using Incremental Unknowns, presenting steady solutions for Reynolds number (Re) up to 7500 with a maximum grid size of 256×256.

Bruneau and Jouron [1] employed a full multigrid-full approximation storage (FMG-FAS) method to solve the Navier-Stokes equations in primitive variables. They achieved steady solutions with a grid size of 256×256 for Reynolds number (Re) up to 5000. Grigoriev and Dargush [12] introduced a sparse boundary element method (BEM) for simulating steady non-uniformly heated viscous fluid flow. They enhanced the penalty function technique by employing hexagonal subregions and discretized the integral equation for each subregion. A non-uniform mesh consisting of 5040 quadrilateral cells was utilized, enabling them to successfully model driven cavity flow up to $Re = 5000$. Demir and Erturk [5] conducted a numerical investigation of the wall driven flow of a viscoelastic fluid within a rectangular cavity. Erturk et al. [6] presented a proficient numerical approach for modeling driven cavity flow through the utilization of the stream function and vorticity formulation. They applied a grid resolution of 601×601 and addressed the Navier-Stokes equations for Reynolds numbers (Re) ranging up to 21000.

Building on the motivation from [6], this study is primarily centered on deriving numerical solutions for the steady, incompressible dilatant flow occurring within an enclosed cavity region. The relationship between velocity and pressure is articulated through the vorticity-stream function correlation, with particular emphasis placed on the treatment of boundary conditions. Computational analyses are conducted across a spectrum of Reynolds numbers, scrutinizing their impact on the flow structure. The characteristics and stability of cavity flow are thoroughly examined.

2. Numerical Method

This section presents the numerical method used herein. The schematic diagram of the problem in a closed cavity region is presented in Figure 1:

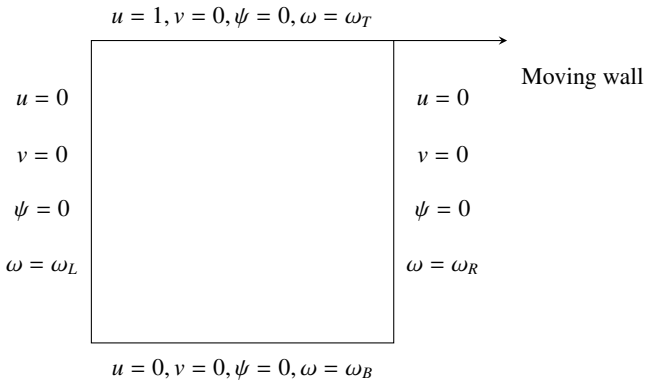

Figure 1. Physical configuration of boundary conditions

We employ the stream function (ψ) and vorticity (ω) formulation for representing the steady-state, incompressible dilatant viscous fluid equations, as follows:

$$u\frac{\partial\omega}{\partial x}+v\frac{\partial\omega}{\partial y}=\frac{1}{\mathrm{Re}\eta(q)}\left\{\frac{\partial}{\partial x}\left(\eta^2(q)\frac{\partial\omega}{\partial x}\right)+\frac{\partial}{\partial y}\left(\eta^2(q)\frac{\partial\omega}{\partial y}\right)\right\} + \frac{1}{\mathrm{Re}}\left\{-4\frac{\partial^2\psi}{\partial x\partial y}\frac{\partial^2\eta(q)}{\partial x\partial y}-\left(\frac{\partial^2\psi}{\partial y^2}-\frac{\partial^2\psi}{\partial x^2}\right)\left(\frac{\partial^2\eta(q)}{\partial y^2}-\frac{\partial^2\eta(q)}{\partial x^2}\right)\right\}, \tag{2.1}$$

$$\frac{\partial^2\psi}{\partial x^2}+\frac{\partial^2\psi}{\partial y^2}=-\omega, \tag{2.2}$$

$$u=\frac{\partial\psi}{\partial y}\,,\quad v=-\frac{\partial\psi}{\partial x},$$

where, $\mathrm{Re}=\frac{\rho\mathrm{VL}}{\eta(0)}$ is the Reynolds number, $\eta(q)$ is the viscosity, q is the shear rate, and x and y are the Cartesian coordinates. In this work, the Cross model is applied to characterize the viscosity function, expressed as:

$$\eta\left(q\right)=\eta\left(\infty\right)+\frac{\eta\left(0\right)-\eta\left(\infty\right)}{1+\left(\lambda q\right)^{1-n}}$$

. In the context of the Cross Model, $\eta(\infty)$ represents the infinite shear viscosity for situations involving very high deformation rates, while $\eta(0)$ characterizes the zero-shear rate viscosity for very low rates of shear. Under the presumption of specific values, such as $n=0.5\,,\lambda=1\,,\eta(\infty)=1$ and within the range $0\leq\eta(0)\leq 1$, this model yields the description of shear-thickening, often referred to as dilatant behavior. Pseudo-time derivatives of the first order are now incorporated into Equations (2.1) and (2.2) as follows:

$$\frac{\partial\omega}{\partial t}=-\frac{\partial\psi}{\partial y}\frac{\partial\omega}{\partial x}+\frac{\partial\psi}{\partial x}\frac{\partial\omega}{\partial y}+\frac{1}{\mathrm{Re}\eta(q)}\left\{\frac{\partial}{\partial x}\left(\eta^2(q)\frac{\partial\omega}{\partial x}\right)+\frac{\partial}{\partial y}\left(\eta^2(q)\frac{\partial\omega}{\partial y}\right)\right\} + \frac{1}{\mathrm{Re}}\left\{-4\frac{\partial^2\psi}{\partial x\partial y}\frac{\partial^2\eta(q)}{\partial x\partial y}-\left(\frac{\partial^2\psi}{\partial y^2}-\frac{\partial^2\psi}{\partial x^2}\right)\left(\frac{\partial^2\eta(q)}{\partial y^2}-\frac{\partial^2\eta(q)}{\partial x^2}\right)\right\}, \tag{2.3}$$

$$\frac{\partial\psi}{\partial t}=\frac{\partial^2\psi}{\partial x^2}+\frac{\partial^2\psi}{\partial y^2}+\omega. \tag{2.4}$$

By applying a forward difference approximation to the time derivatives in Equations (2.3) and (2.4), we can rearrange the equations as follows:

$$\left(1-\frac{\Delta t}{\mathrm{Re}}\eta^n\frac{\partial^2}{\partial x^2}+\Delta t\left(\frac{\partial\psi}{\partial y}\right)^n\frac{\partial}{\partial x}-2\frac{\Delta t}{\mathrm{Re}}\left(\frac{\partial\eta}{\partial x}\right)^n\frac{\partial}{\partial x}\right)\left(1-\frac{\Delta t}{\mathrm{Re}}\eta^n\frac{\partial^2}{\partial y^2}-\Delta t\left(\frac{\partial\psi}{\partial x}\right)^n\frac{\partial}{\partial y}-2\frac{\Delta t}{\mathrm{Re}}\left(\frac{\partial\eta}{\partial y}\right)^n\frac{\partial}{\partial y}\right)\omega^{n+1} = \omega^n+\frac{\Delta t}{\mathrm{Re}}\left\{-4\left(\frac{\partial^2\psi}{\partial x\partial y}\right)^n\left(\frac{\partial^2\eta}{\partial x\partial y}\right)^n-\left[\left(\frac{\partial^2\psi}{\partial y^2}\right)^n-\left(\frac{\partial^2\psi}{\partial x^2}\right)^n\right]\times\left[\left(\frac{\partial^2\eta}{\partial y^2}\right)^n-\left(\frac{\partial^2\eta}{\partial x^2}\right)^n\right]\right\}, \tag{2.5}$$

$$\left(1-\Delta t\frac{\partial^2}{\partial x^2}\right)\left(1-\Delta t\frac{\partial^2}{\partial y^2}\right)\psi^{n+1}=\psi^n+\Delta t\omega^n. \tag{2.6}$$

Upon reaching a steady state, we have

$$\psi^{n+1}=\psi^n$$

and

$$\omega^{n+1}=\omega^n.$$

By substituting this result into the right-hand side of Equations (2.5) and (2.6), we can express as:

$$\left(1-\frac{\Delta t}{\mathrm{Re}}\eta^n\frac{\partial^2}{\partial x^2}+\Delta t\left(\frac{\partial\psi}{\partial y}\right)^n\frac{\partial}{\partial x}-2\frac{\Delta t}{\mathrm{Re}}\left(\frac{\partial\eta}{\partial x}\right)^n\frac{\partial}{\partial x}\right)\left(1-\frac{\Delta t}{\mathrm{Re}}\eta^n\frac{\partial^2}{\partial y^2}-\Delta t\left(\frac{\partial\psi}{\partial x}\right)^n\frac{\partial}{\partial y}-2\frac{\Delta t}{\mathrm{Re}}\left(\frac{\partial\eta}{\partial y}\right)^n\frac{\partial}{\partial y}\right)\omega^{n+1} = \omega^n+\frac{\Delta t}{\mathrm{Re}}\left\{-4\left(\frac{\partial^2\psi}{\partial x\partial y}\right)^n\left(\frac{\partial^2\eta}{\partial x\partial y}\right)^n-\left[\left(\frac{\partial^2\psi}{\partial y^2}\right)^n-\left(\frac{\partial^2\psi}{\partial x^2}\right)^n\right]\times\left[\left(\frac{\partial^2\eta}{\partial y^2}\right)^n-\left(\frac{\partial^2\eta}{\partial x^2}\right)^n\right]\right\}, \tag{2.7}$$

$$+\left(\frac{\Delta t}{\mathrm{Re}}\eta^n\frac{\partial^2}{\partial x^2}-\Delta t\left(\frac{\partial\psi}{\partial y}\right)^n\frac{\partial}{\partial x}+2\frac{\Delta t}{\mathrm{Re}}\left(\frac{\partial\eta}{\partial x}\right)^n\frac{\partial}{\partial x}\right)\times\left(\frac{\Delta t}{\mathrm{Re}}\eta^n\frac{\partial^2}{\partial y^2}+\Delta t\left(\frac{\partial\psi}{\partial x}\right)^n\frac{\partial}{\partial y}+2\frac{\Delta t}{\mathrm{Re}}\left(\frac{\partial\eta}{\partial y}\right)^n\frac{\partial}{\partial y}\right)\omega^n$$

$$\left(1-\Delta t\frac{\partial^2}{\partial x^2}\right)\left(1-\Delta t\frac{\partial^2}{\partial y^2}\right)\psi^{n+1}=\psi^n+\Delta t\omega^n+\left(\Delta t\frac{\partial^2}{\partial x^2}\right)\left(\Delta t\frac{\partial^2}{\partial y^2}\right)\psi^n. \tag{2.8}$$

The solution method for Equations (2.7) and (2.8) employs a two-level updating process. Initially, we solve the stream function equation. We now introduce the variable f in Equation (2.8). It plays a crucial role in this approach, as follows:

$$\left(1-\Delta t\frac{\partial^2}{\partial y^2}\right)\psi^{n+1}=f \tag{2.9}$$

and

$$\left(1-\Delta t\frac{\partial^2}{\partial x^2}\right)f=\psi^n+\Delta t\omega^n+\left(\Delta t\frac{\partial^2}{\partial x^2}\right)\left(\Delta t\frac{\partial^2}{\partial y^2}\right)\psi^n \tag{2.10}$$

In Equation (2.10), f is the only unknown. It is first solved at each grid point. Subsequently, the stream function variable (ψ) is moved to the new time step by means of Equation (2.9). Then the vorticity equation is solved the same way.

3. Result and Discussion

We apply symmetry to ψ and ω at points located outside the boundaries. Along the boundaries, vorticity values are determined using a nine-point compact finite difference scheme.

Left Boundary

$\psi_{-1,j}=\psi_{1,j}\,,\ \psi_{0,j}=0$

$u=v=0$

$\omega_{0,j}=-\left(\dfrac{\partial^2\psi}{\partial x^2}\right)_{0,j}$

Right Boundary

$\psi_{N+1,j}=\psi_{N-1,j}\,,\ \psi_{N,j}=0$

$u=v=0$

$\omega_{N,j}=-\left(\dfrac{\partial^2\psi}{\partial x^2}\right)_{N,j}$

Bottom Boundary

$\psi_{i,-1}=\psi_{i,1}\,,\ \psi_{i,0}=0$

$u=v=0$

$\omega_{i,0}=-\left(\dfrac{\partial^2\psi}{\partial y^2}\right)_{i,0}$

Top Boundary

$\psi_{i,N+1}=\psi_{i,N-1}\,,\ \psi_{i,N}=0$

$u=1\,,v=0$

$\omega_{i,N}=-\left(\dfrac{\partial^2\psi}{\partial y^2}\right)_{i,N}$

Our convergence criterion is different from that of Erturk et al. [6], although we use the same algorithm. Specifically, our convergence criterion is based on the relative-error criteria, for all n,

$$\max\left\{\frac{\left|\psi^{n+1}-\psi^n\right|}{1+|\psi^n|}\right\}<10^{-6}$$

and

$$\max\left\{\frac{\left|\omega^{n+1}-\omega^n\right|}{1+|\omega^n|}\right\}<10^{-6}.$$

TABLE 1. Comparison of the properties of the primary vortex; the maximum value of the stream function, the value of the vorticity and the location of the centre, for a Newtonian fluid at $Re = 1000$

Reference	Grid	ψ	ω	x	y
Erturk et al. [6]	401×401	0.118585	2.062761	0.5300	0.5650
	513×513	0.118722	2.064765	0.5313	0.5645
	601×601	0.118781	2.065530	0.5300	0.5650
Wright and Gaskell [20]	1024×1024	0.118821	2.06337	0.5308	0.5659
Nishida and Satofuka [16]	129×129	0.119004	2.068546	0.5313	0.5625
Goyon [11]	129×129	0.1157	-	0.5312	0.5625
Bruneau and Jouran [1]	256×256	0.1163	-	0.5313	0.5586
Grigoriev and Dargush [12]	-	0.11925	-	0.531	0.566
Present	128×128	0.115952	2.02482	0.5313	0.5625
	256×256	0.118182	2.05677	0.5313	0.5664
	401×401	0.118626	2.06322	0.5312	0.5661

In Table 1, the maximum value of the stream function, the value of the vorticity at the centre of the primary vortex and the position of the centre of the primary vortex for a Newtonian fluid at $Re = 1000$, are tabulated and compared with similar results found in the literature. Erturk et al. [6] solved the cavity flow on three different grid meshes ($401 \times 401, 513 \times 513, and\, 601 \times 601$) for $Re = 1000$ as one of the most important results in Table 1. Referring to Table 1, it's evident that our results at $Re = 1000$ exhibit strong agreement with the findings of Bruneau and Jouran [1], Goyon [11], and Erturk et al. [6]. Based on these comparative findings, it can be deduced that, even at $Re = 1000$, achieving accuracy requires higher-order approximations in conjunction with the use of fine grids.

We initiated the computations by solving the driven cavity flow for dilatant fluids, covering the range from $Re = 1000$ to $Re = 3000$. Figures 2-4 represent the results: In Figure 2, with the grid size of 128×128, obtaining a steady solution for $Re = 5000$ might be challenging. Therefore, in Figure 3, we attempted to resolve the $Re = 5000$ case using a larger grid size of 256×256, which led to a successful acquisition of a steady solution. It was then decided to increase the number of grids, and we tried to solve the same Reynolds numbers with 401×401 grids in Figure 4. Once again, we were able to achieve a steady solution. The figures above have shown that the secondary vortices appear at the corners as the Reynolds number increases.

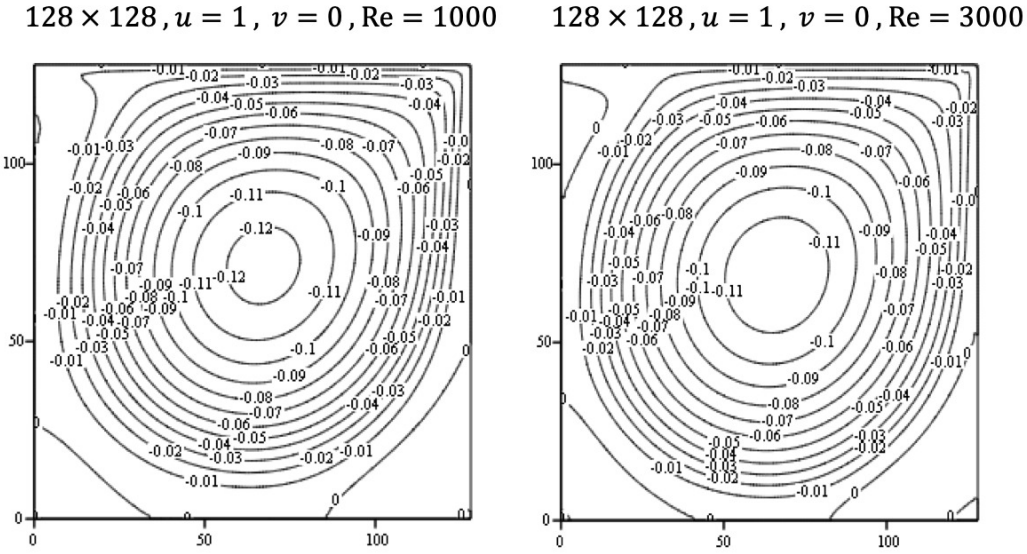

FIGURE 2. Streamline contours for dilatant fluids at $Re = 1000$ and $Re = 3000$, respectively

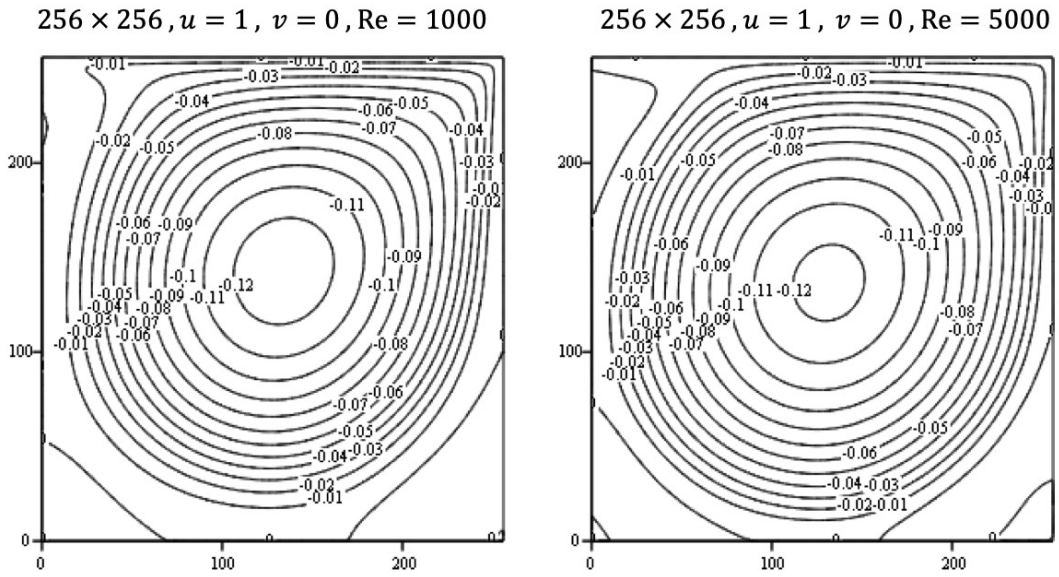

FIGURE 3. Streamline contours for dilatant fluids at $Re = 1000$ and $Re = 5000$, respectively

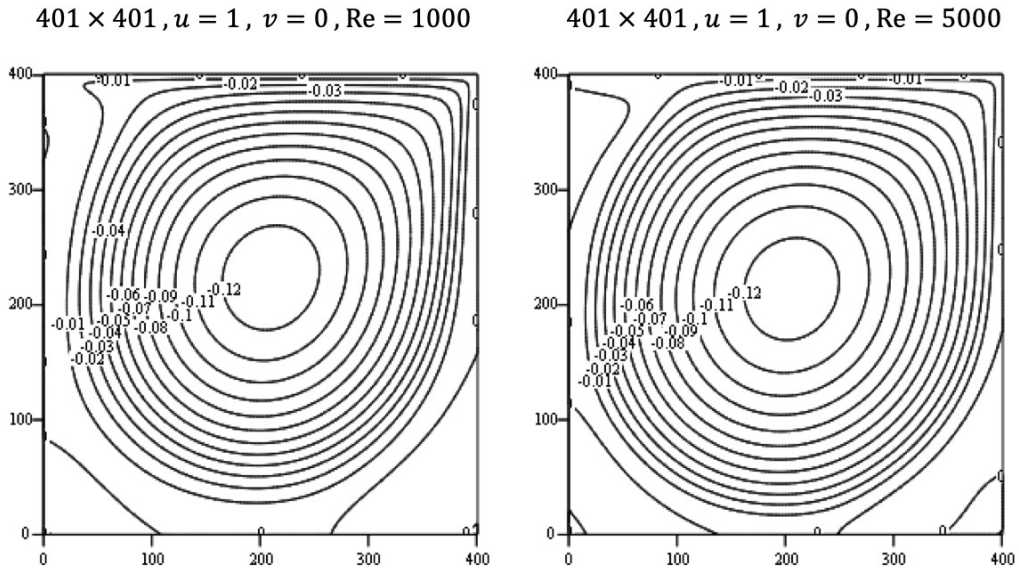

FIGURE 4. Streamline contours for dilatant fluids at $Re = 1000$ and $Re = 5000$, respectively

4. CONCLUSION

In this study, numerical solutions have been presented and documented for the steady 2D incompressible dilatant flow in a closed cavity region for Reynolds numbers up to $Re = 5000$. The continuity and momentum equations have been solved using pseudo time derivative approach considering appropriate initial and boundary conditions. Then, the equations governing flow motion have been decomposed using the finite difference method and subsequently solved numerically for dilatant fluids. Each equation within the numerical formulation demands solving two tridiagonal systems. This characteristic enables the straightforward use of large grid meshes, and we have employed a fine grid mesh with dimensions of 401×401. The method has demonstrated exceptional effectiveness, particularly in addressing flow problems demanding high accuracy and using very fine grid meshes [7, 8]. The computations highlight the necessity of employing a fine grid mesh to achieve a steady solution. Additionally, as the Reynolds number (Re)

increases, secondary vortices emerge, particularly at the corners. Based on these comparative analyses, it is evident that achieving accuracy, even at $Re = 1000$, requires higher-order approximations in conjunction with the utilization of fine grids. In future studies, researchers can investigate whether it is possible to perform steady-state computations of driven cavity flow beyond $Re = 5000$ with grid sizes larger than 401×401.

Conflicts of Interest

The author/authors declare that there are no conflicts of interest regarding the publication of this article.

Authors Contribution Statement

The author has read and agreed the published version of the manuscript.

References

[1] Bruneau, C.H., Jouron, C., *An efficient scheme for solving Steady incompressible Navier–Stokes equations*, Journal of Computational Physics, **89**(1990), 389–413.

[2] Burggraf, O., *Analytical and numerical studies of the structure of Steady separated flows*, Journal of Fluid Mechanics, **24**(1966), 113–151.

[3] Chhabra, R., Richardson, J., Non-Newtonian Flow and Applied Rheology: Engineering Applications, 2nd Edition, Butterworth-Heinemann: Oxford, 2008.

[4] Coussot, P., *Yield stress fluid flows: A review of experimental data*, Journal of Non-Newtonian Fluid Mechanics, **211**(2014), 31–49.

[5] Demir, H., Erturk, V.S., *A numerical study of wall driven flow of a viscoelastic fluid in rectangular cavities*, Indian Journal of Pure and applied Mathematics, **32**(2001), 1581–1590.

[6] Erturk, E., Corke, T.C., Gökçöl, C., *Numerical solutions of 2-D Steady incompressible driven cavity flow at high Reynolds numbers*, International Journal for Numerical Methods in Fluids, **48**(2005), 747–774.

[7] Erturk, E., Corke, T.C., *Boundary layer leading-edge receptivity to sound at incidence angles*, Journal of Fluid Mechanics, **444**(2001), 383–407.

[8] Erturk, E., Haddad, O.M., Corke, T.C., *Laminar incompressible flow past parabolic bodies at angles of attack*, American Institute of Aeronautics and Astronautics Journal, **42**(2004), 2254–2265.

[9] Gangawane, K.M., Manikandan, B., *Laminar natural convection characteristics in an enclosure with heated hexagonal block for non-Newtonian power law fluids*, Chinese Journal of Chemical Engineering, **25**(2017), 555–571.

[10] Ghia, U., Ghia, K.N., Shin, C.T., *High-Re solutions for incompressible flow using the Navier-Stokes equations and a multigrid method*, Journal of Computational Physics, **48**(1982), 387–411.

[11] Goyon, O., *High-Reynolds number solutions of Navier–Stokes equations using incremental unknowns*, Computer Methods in Applied Mechanics and Engineering, **130**(1996), 319–335.

[12] Grigoriev, M.M., Dargush, G.F., *A Poly-Region boundary element method for incompressible viscous fluid flows*, International Journal for Numerical Methods in Engineering, **46**(1999), 1127–1158.

[13] Khorasanizade, S., Sousa, J.M., *A detailed study of Lid-drivencavity flow at moderate Reynolds numbers using incompressible SPH*, International Journal for Numerical Methods in Fluids, **76**(2014), 653–668.

[14] Lu, G., Wang, X.D., Duan, Y.Y., *A critical review of dynamic wetting by complex fluids: From Newtonian Fluids to Non-Newtonian Fluids and Nanofluids*, Advances in Colloid and Interface Science, **236**(2016), 43–62.

[15] Mahmood, R., Bilal, S., Khan, I., Kousar, N., Seikh, A.H. et al., *A Comprehensive finite element examination of Carreau Yasuda fluid model in a Lid driven cavity and channel with obstacle by way of kinetic energy and drag and lift coefficient measurements*, Journal of Materials Research and Technology, **9**(2020), 1785–1800.

[16] Nishida, H., Satofuka, N., *Higher-order solutions of square driven cavity flow using a variable-order multi-grid method*, International Journal for Numerical Methods in Fluids, **34**(1992), 637–653.

[17] Shenoy, A., Heat Transfer to Non-Newtonian Fluids: Fundamentals and Analytical Expressions, Wiley-VCH: Weinheim, 2018.

[18] Shuguang, L., *Numerical simulation of non-Newtonian carreau fluid in a Lid driven cavity*, Journal of Physics: Conference Series, **2091**(2021), 012068.

[19] Sivakumar, P., Bharti, R.P., Chhabra, R.P., *Steady flow of power-law fluids across an unconfined elliptical cylinder*, Chemical Engineering Science, **62**(2007),1682–1702.

[20] Wright, N.G., Gaskell, P.H., *An efficient multigrid approach to solving highly recirculating flows*, Computers and Fluids, **24**(1995), 63–79.

[21] Xu, H., Liao, S.J., *Laminar flow and heat transfer in the boundary-layer of non-Newtonian fluids over a stretching flat sheet*, Computers & Mathematics with Applications, **57**9(2009), 1425–1431.

[22] Xu, R., Stansby, P., Laurence, D., *Accuracy and stability in incompressible SPH(ISPH) based on the projection method and a new approach*, Journal of Computational Physics, **228**(2009), 6703–6725.